Have Optical Wigner's Friend Experiments Been Blind to a Geometric Degree of Freedom?

VietVunVut (Viet – Nguyen Xuan)[1, *]
[1] *Independent Researcher, Vietnam*
(Dated: 2026-05-31)

The two published optical Wigner's Friend experiments have operated exclusively at an equatorial measurement geometry ($\theta = \pi/2$) — a fixed point where every overlap-dependent deformation of quantum measurement statistics vanishes identically (Proposition 1, equatorial cancellation theorem). A single waveplate breaks this cancellation. Re-inserting one quarter-wave plate into the Bong et al. (2020) apparatus tilts the Superobserver measurement to $\theta = 31°$, providing minimum detectable $\beta \sim 0.075$ at 5σ (single-setting) — a search parameter whose methodological role parallels SME coefficients [15] (§II C) — while preserving the Genuine LF violation (8.6σ). A complete survey (Supplemental S1) finds no published implementation has varied this polar angle; only two exist (Proietti 2019, Bong 2020). The theorem constrains the overlap-only class; broader deformation classes (Levels 1–3, §III D) lie outside its scope. Under fair-sampling ($\eta \approx 0.87$), this is a loophole-open screening test; a null $\delta\langle AB\rangle$ across a full θ-sweep would falsify the overlap-only class.

I. INTRODUCTION

Extended Wigner's Friend (EWF) experiments [1, 2] test whether observed events exist independently of who observes them. Modern optical implementations combining Local Friendliness (LF) no-go theorems [2, 10, 11] have challenged the absoluteness of observed events [13, 14].

In brief. Every published optical EWF experiment has used — by convention for LF optimization, not by design — the one measurement geometry ($\theta = \pi/2$) at which an entire class of overlap-dependent quantum deformations cancels identically. A single waveplate breaks this accidental fixed point, enabling the first experimental probe of this class. The predicted signal $\delta\langle AB\rangle$ vanishes identically at $\theta = \pi/2$ and is generically nonzero otherwise — a genuine observable, not a coordinate artifact (Lemma 1, §III C). The paper's contribution is twofold: a geometric null theorem (Proposition 1) showing that equatorial measurements leave the overlap-only class systematically unexplored, and a single-waveplate protocol (§IV–VII) enabling its first experimental test. This paper makes no claim about the existence of overlap-dependent deformation in nature — it proposes a null-test protocol analogous in method to the Standard Model Extension [15] (§II C).

Proposition 1 (Equatorial Cancellation Theorem, §III). A deformation of quantum measurement statistics is *overlap-only* if the modified joint probability takes the form $P'(a, b|x, y) = P_{\mathrm{QM}}(a, b|x, y) \cdot g(|\langle b|d\rangle|^2)/Z$, for any function $g : [0, 1] \to \mathbb{R}$ and normalization Z. At the equatorial plane ($\theta = \pi/2$), $|\langle b|d\rangle|^2 = 1/2$ for all outcome pairs (b, d); hence $g(|\langle b|d\rangle|^2)$ is constant and $P' = P_{\mathrm{QM}}$ identically — the equator is a geometric null point for every overlap-only deformation. The signal $\delta\langle AB\rangle(\theta)$ is invariant under any basis redefinition (Lemma 1, §III C).

Breaking the cancellation requires only a single quarter-wave plate: re-inserting the QWP into the Bong et al. (2020) apparatus tilts the Superobserver measurement to $\theta = 31°$, providing minimum detectable $\beta \sim 0.075$ at 5σ (single-setting) while preserving 8.6σ Genuine LF violation (§IV–VII).

Its two claims are structural: (A) within surveyed optical EWF implementations (Supplemental S1), equatorial measurement — a convention for LF optimization, not a tested constraint — leaves the overlap-only class systematically unexplored, and (B) a single waveplate enables the first experimental probe of this class. Positive results require independent verification including θ-sweeps (§VIII).

Supplemental material: S1 (literature search + algebraic proof), S2 (numerical methods + statistical robustness).

II. BACKGROUND

A. Extended Wigner's Friend Setup

Bong et al. (2020) [2] used two entangled photon pairs produced by spontaneous parametric down-conversion (SPDC) at 810 nm. On each side, a Friend measures photon polarization in the z-basis inside an interferometric lab formed by beam displacers. A Superobserver measures the combined Friend+photon system at three settings: Setting 1 (z-basis, reads the Friend outcome directly); Settings 2 and 3 (azimuthal angles on the Bloch sphere equator, $\theta = \pi/2$). Measurement outcomes are binary, $a, b \in \{+1, -1\}$, with $N = 91{,}000$ coincidences per setting.

[Schematic of the EWF setup with tilted Superobserver measurement is provided in Supplemental S1.]

* viet@vvvqmrf.com; https://vvvqmrf.com

B. Genuine Local Friendliness Inequality

The Genuine Local Friendliness Facet 1 inequality [2] is:

$$\text{Gen LF } 1 = -\langle A_1\rangle - \langle A_2\rangle - \langle B_1\rangle - \langle B_2\rangle - \langle A_1B_1\rangle - 2\langle A_1B_2\rangle - 2\langle A_2B_1\rangle + 2\langle A_2B_2\rangle - \langle A_2B_3\rangle - \langle A_3B_2\rangle - \langle A_3B_3\rangle - 6 \leq 0 \tag{1}$$

A violation rules out all theories satisfying Local Friendliness.

C. Overlap-Dependent Deformation: Why This Class?

Definition and motivation. The basis overlap $|\langle b|d\rangle|^2$ is the simplest scalar quantifying the geometric relationship between two measurement bases. Any deformation coupling Superobserver statistics to a prior observer's recorded outcome must depend on this relationship at lowest order; the overlap-only class is therefore the minimal operational deformation — it isolates the geometric degree of freedom (θ) that equatorial measurements leave systematically unexplored.

Consider modifications to quantum probabilities:

$$P(a,b \mid x,y) = P_{\mathrm{QM}}(a,b \mid x,y)\cdot[1-\beta\cdot g(b,\text{Friend outcome})]/Z \tag{2}$$

where $\beta \in [0,1]$; $\beta = 0$ recovers standard QM. Three constraints — (i) rotation invariance, (ii) alignment limit $g(1) = 0$, (iii) monotonicity — force the leading-order expansion $g(x) = c_1(1-x) + O((1-x)^2)$. Adopting the simplest representative and absorbing c_1 into β:

$$f_\perp(b,d) = 1 - |\langle b|d\rangle|^2, \tag{3}$$

where $b \in \{+1,-1\}$ is the Superobserver outcome and $d \in \{H,V\}$ is the Friend outcome. The functional form Eq. (3) is the simplest satisfying (i)–(iii); every smooth function obeying them shares the same first-order structure $g(x) \propto (1-x)$. The equatorial cancellation theorem (§III) constrains every overlap-dependent deformation independent of parametrization — it holds for any function $g(|\langle b|d\rangle|^2)$.

Within the broader deformation hierarchy (§III D), Level 0 is prioritized: (i) it is the only level with a sharp geometric null (Proposition 1), providing a built-in control; (ii) it requires only a single waveplate. This prioritization is methodological, not predictive — the experiment tests whether nature exhibits overlap-dependent deformation.

Methodological role. Equation (2) is a benchmark parametrization — a phenomenological ansatz, not derived from any underlying physical theory. No existing theory predicts this specific form. The parametrization functions analogously to SME coefficients [15]: the SME was proposed with 19 coefficients and no a priori predictions, yet progressively tighter null results constrained previously unconstrained parameter space. The overlap-only parametrization serves the identical methodological function — β is a search parameter whose null result constrains new parameter space at the $\sim 10^{-2}$ scale. Operationally, β is directly measurable via $\delta\langle AB\rangle$ at any $\theta \neq \pi/2$, with the θ-dependent variation under θ-sweep (§VIII) providing the distinguishing signature (vanishing identically at $\theta = \pi/2$ and determined numerically otherwise) that separates an overlap-dependent signal from conventional systematics.

Null test. The experiment is a null test: standard QM predicts the same LF violation regardless of θ; a θ-dependent signal would indicate a departure from standard QM independently of model class.

III. EQUATORIAL CANCELLATION THEOREM (CLAIM A)

A. Main Result (Model-Independent)

Let a Friend F measure in the z-basis ($\{|H\rangle, |V\rangle\}$) and a Superobserver W measure at Bloch sphere angles (θ,ϕ). With $f_\perp(b,d) = 1 - |\langle b|d\rangle|^2$:

$$f_\perp(+1,H) - f_\perp(-1,H) = -\cos\theta. \tag{4}$$

Consequently, $f_\perp$ is overlap-independent if and only if $\theta = \pi/2$. For any equatorial Superobserver measurement, any model of the form Eq. (2)–(3) reduces exactly to standard quantum mechanics, regardless of the deformation strength β. This depends only on Bloch sphere geometry. Eq. (2)–(3) serves only to quantify experimental sensitivity (§V C); the theorem holds for any overlap function. The experimental consequence is that equatorial measurements cannot distinguish standard QM from any overlap-dependent deformation within this class. The distinctive experimental signature is that $\delta\langle AB\rangle$ vanishes identically at $\theta = \pi/2$ and is generically non-zero for $\theta \neq \pi/2$ (exact θ-dependence determined numerically, §V C): this structure is distinct from conventional systematics (which either cancel in $\delta\langle AB\rangle$ or produce non-geometric θ-dependence) and is a genuine observable, not a gauge artifact (Lemma 1, §III C).

B. Equatorial Cancellation Theorem

Definition (Overlap-only class). A deformation of quantum measurement statistics is *overlap-only* if the modified joint probability takes the form $P'(a,b \mid x,y) = P_{\mathrm{QM}}(a,b \mid x,y)\cdot g(|\langle b|d\rangle|^2)/Z$, where $g : [0,1] \to \mathbb{R}$ is any function and $Z = \sum_{a,b} P_{\mathrm{QM}}(a,b \mid x,y)\cdot g(|\langle b|d\rangle|^2)$ normalizes the distribution.

Proposition 1 (Equatorial Cancellation Theorem). Let g be any function. At $\theta = \pi/2$, $|\langle b|d\rangle|^2 = 1/2$ for all outcome pairs (b,d). Hence $g(|\langle b|d\rangle|^2) = g(1/2)$ is constant, and $P'(a,b \mid x,y) = P_{\mathrm{QM}}(a,b \mid x,y)$. The

equatorial plane is a fixed point of every overlap-only deformation; no overlap-dependent modification evades this cancellation while depending only on $|\langle b|d\rangle|^2$. □

C. Lemma 1 (Non-Absorption)

Lemma 1 (Non-Absorption). The $\cos\theta$ term in Eq. (4) cannot be absorbed by unitary redefinition of the Superobserver's measurement basis.

Proof. Throughout, $\delta\langle AB\rangle \equiv \langle AB\rangle_{\text{model}} - \langle AB\rangle_{\text{QM}}$ denotes the deviation of the deformed model from standard QM (the same quantity tabulated in §V C), not a bare correlator value. Two distinct operations must be distinguished. (i) *Passive relabeling*: redefining outcome labels via $|b'\rangle = U|b\rangle$ is a change of description, not a change of the measurement — it acts identically on the deformed model and on standard QM. It therefore cannot generate any model–QM deviation: $\delta\langle AB\rangle = 0$ identically for any U and any θ. (ii) *Active physical rotation*: changing the measurement axis $(\theta, \phi) \to (\theta', \phi')$ physically reorients the apparatus, altering the overlap $|\langle b|d\rangle|^2$. Eq. (2) couples to this physical overlap, which depends on the Friend outcome d — a degree of freedom external to the Superobserver's basis choice. The $\cos\theta$ term in Eq. (4) is a function of the physical angle θ, not of the basis labels; it cannot be removed by any relabeling U because relabeling does not change θ. Passive relabeling predicts $\delta\langle AB\rangle = 0$ for all θ and U; Eq. (2) predicts $\delta\langle AB\rangle \neq 0$ for $\theta \neq \pi/2$. The two are operationally distinct. □

Numerical illustration. At $\theta = 31^\circ$ with $\beta = 0.07$, the overlap-only model predicts $\delta\langle AB\rangle \approx 0.008$ (4.7σ at $N = 91{,}000$). Any unitary relabeling of the Superobserver basis — e.g., swapping $|+1\rangle \leftrightarrow |-1\rangle$ via $U = \sigma_x$ — flips the sign of each individual correlator ($\langle AB\rangle \to -\langle AB\rangle$) but acts identically on the model and on QM, leaving their difference at zero ($\delta\langle AB\rangle = 0$); Eq. (2), by contrast, still predicts a nonzero deviation $\delta\langle AB\rangle \approx 0.008$. The two predictions are numerically and operationally distinct.

Operational invariant. $\delta\langle AB\rangle_\theta = \langle AB\rangle_\theta - \langle AB\rangle_{\pi/2}$ is invariant under any unitary transformation on the Superobserver's Hilbert space alone — it cannot be eliminated by any choice of measurement coordinates. Only $\beta = 0$ (standard QM) or $\theta = \pi/2$ (equatorial measurement) removes it. Any non-zero $\delta\langle AB\rangle$ at $\theta \neq \pi/2$ therefore indicates departure from the standard Born rule, independent of measurement-basis convention.

D. Scope Limitation

The overlap-only class is the minimal phenomenological class capturing dependence on $|\langle b|d\rangle|^2$; we do not claim completeness over all possible deformations. Proposition 1 constrains deformations whose modification factor depends solely on $|\langle b|d\rangle|^2$. Broader deformations — depending on the full reduced density matrix ρ_F of the Friend (rather than only $|\langle b|d\rangle|^2$), on the concurrence between Friend and Superobserver subsystems, or on non-geometric variables such as timing or path — lie outside this theorem's scope. For instance, a deformation $P' \propto P_{\text{QM}} \cdot h(\text{Tr}[\rho_F^2])$ would depend on Friend state purity, not basis overlap, and would not cancel at the equator. The experiment (§IV–VII) constrains the overlap-only class (Level 0 of a natural hierarchy: Level 1 — density-matrix-dependent; Level 2 — multi-partite; Level 3 — non-geometric). Each level beyond 0 is unconstrained by Proposition 1 and requires independent designs.

Contextuality distinction. Overlap-dependence is logically independent of standard KS contextuality — it concerns measurement *record* (geometric relationship to a prior outcome), not measurement *setting* (which observables are measured jointly). Proposition 1 constrains the former and is silent on the latter.

TABLE I. Distinction between KS contextuality, overlap-dependence, and weak measurement.

Property	KS Contextuality	Overlap-Dependence (this work)	Weak Measurement [18]
Depends on	Measurement setting	Recorded outcome (geometric relationship to prior outcome)	Postselection choice
Observable	Outcome distributions across incompatible settings	$\delta\langle AB\rangle(\theta)$ vanishing iff $\theta = \pi/2$, at fixed setting	Weak value A_w
Constrained by	Bell-KS inequalities	Proposition 1 (equatorial cancellation)	—

E. Proof

The Superobserver measurement basis at (θ, ϕ):

$$|b = +1\rangle = \cos(\theta/2)|H\rangle + e^{i\phi}\sin(\theta/2)|V\rangle, \tag{5}$$

$$|b = -1\rangle = \sin(\theta/2)|H\rangle - e^{i\phi}\cos(\theta/2)|V\rangle. \tag{6}$$

Squared overlaps (ϕ drops out: $|e^{i\phi}|^2 = 1$):

$$|\langle b = +1|H\rangle|^2 = \cos^2(\theta/2), \qquad |\langle b = +1|V\rangle|^2 = \sin^2(\theta/2), \tag{7}$$

$$|\langle b = -1|H\rangle|^2 = \sin^2(\theta/2), \qquad |\langle b = -1|V\rangle|^2 = \cos^2(\theta/2). \tag{8}$$

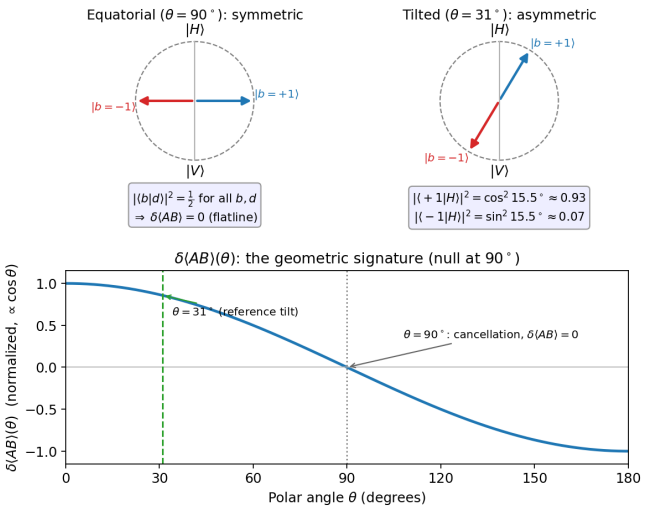

FIG. 1. **Equatorial flatline vs. tilted $\cos\theta$ emergence.** Left panel: Bloch sphere showing Superobserver measurement axis at equator ($\theta = \pi/2$). All four overlap magnitudes $|\langle b|d\rangle|^2 = 1/2$ — symmetric, balanced, $\delta\langle AB\rangle = 0$ identically (flatline). Right panel: axis tilted to $\theta = 31°$. Overlap asymmetry emerges: $|\langle +1|H\rangle|^2 = \cos^2(15.5°) \approx 0.93$, $|\langle -1|H\rangle|^2 = \sin^2(15.5°) \approx 0.07$ — the Superobserver basis aligns preferentially with one Friend outcome. Lower panel: predicted $\delta\langle AB\rangle(\theta)$ curve (numerical), showing the exact null at $\theta = 90°$ (equator) and the onset of non-zero signal as θ departs from the equatorial plane. The single-waveplate modification moves the measurement from the flatline at 90° to the sensitive region at 31° (dashed vertical line).

Overlaps depend only on θ. Computing $f_\perp$:

$$f_\perp(+1, H) = 1 - \cos^2(\theta/2) = \sin^2(\theta/2), \tag{9}$$

$$f_\perp(-1, H) = 1 - \sin^2(\theta/2) = \cos^2(\theta/2), \tag{10}$$

$$f_\perp(+1, H) - f_\perp(-1, H) = -\cos\theta. \tag{11}$$

Vanishes iff $\theta = \pi/2$. All four $f_\perp = 1/2 \to$ constant $\to$ cancels in Z. □

F. Physical Intuition

At $\theta = \pi/2$, the Superobserver's measurement basis is maximally symmetric with respect to the Friend's recorded outcomes: $|\langle b|H\rangle|^2 = |\langle b|V\rangle|^2 = 1/2$ for both $b = \pm 1$ — the Superobserver's measurement apparatus is equally aligned with every Friend record, disturbing both outcomes identically. The overlap is perfectly balanced; no overlap-dependent deformation can produce an asymmetry because there is no asymmetry to amplify.

Tilting to $\theta \neq \pi/2$ breaks this balance: the Superobserver's basis aligns more closely with one Friend outcome (e.g., $|\langle +1|H\rangle|^2 > |\langle +1|V\rangle|^2$ for $\theta < \pi/2$), creating a $\cos\theta$ asymmetry. An overlap-dependent deformation would convert this geometric imbalance into a detectable statistical signal — the measurement apparatus becomes a directional probe for alignment-dependent coupling. Mathematically, such terms are the leading-order expression of any smooth function coupling Superobserver statistics to basis alignment with the Friend outcome; the first-order correction away from perfect alignment generically has the structure $1 - \beta \cdot (1 - |\langle b|d\rangle|^2)$. Eq. (2)–(3) isolates this universal geometric structure without committing to a specific physical mechanism. The experiment (§IV–VII) tests whether nature exploits this asymmetry.

G. An Unisolated Geometric Control Parameter

Survey findings. Only two published optical EWF experiments exist (Supplemental S1): Proietti et al. (2019) and Bong et al. (2020). Both correspond to equatorial symmetry conditions — for Bong et al. this is direct ($\theta = \pi/2$); for Proietti et al. the equivalence follows from the BSM structure (see footnote a).

TABLE II. Published optical EWF experiments: measurement geometry.

Experiment	Year	Measurement	Polar angle θ	Equatorial?
Proietti et al.	2019	BSM (Bell-state)	—[a]	Yes
Bong et al.	2020	Projective (settings 2,3)	$\pi/2$	Yes

[a]BSM projects onto the four Bell states $\{|\Phi^+\rangle, |\Phi^-\rangle, |\Psi^+\rangle, |\Psi^-\rangle\}$. For the singlet-state source used in Proietti et al., each Bell outcome occurs with equal probability and, conditioned on any Bell outcome b, leaves the Friend's recorded outcome equally likely to be H or V: $P(d|b) = 1/2$ for all (b, d) pairs. Because b is a two-photon Bell state and d a single-photon record, the relevant object is this conditional probability, not a single-photon overlap $|\langle b|d\rangle|^2$; the value 1/2 plays the same role here as the equatorial overlap $|\langle b|d\rangle|^2 = 1/2$ derived in §III E, so the BSM configuration is effectively equatorial. Full derivation in Supplemental S1.

Search audit: 4 databases (Google Scholar, arXiv, Web of Science, InspireHEP), Jan 2000–May 2026; Boolean queries combining ("Wigner's friend" OR "extended Wigner") with ("equatorial measurement" OR "Bloch sphere polar angle" OR "outcome dependence" OR "geometric constraint"); ∼200 titles screened → 47 full-text examined → 2 published optical EWF experiments identified (both effectively equatorial; see footnote a). Inclusion criteria: optical EWF implementation with Friend+Superobserver structure, published in peer-reviewed venue or arXiv, reporting measurement settings from which polar angle θ can be determined. Within the surveyed literature, no published EWF experiment varies θ from $\pi/2$. Azimuthal angles are extensively optimized and reported; θ is implicitly fixed to $\pi/2$ without comment. We cannot rule out unpublished results or implementations outside our database scope that may have varied θ. Full query logs in Supplemental S1.

Structural independence from LF optimization. That both surveyed implementations are equatorial fol-

lows directly from the LF optimization convention — it is not an artifact of the small sample. LF inequalities are optimized at equatorial settings [2, 10]; without a hypothesis motivating polar tilt, $\theta = \pi/2$ was adopted as standard and never varied. The LF inequality coefficients (Eq. 1) are structurally independent of θ — the polar angle enters only through correlator values, which are free parameters in any LF test. θ is therefore a genuine independent degree of freedom orthogonal to the LF constraint surface; any EWF experiment on any physical platform (optical, superconducting, trapped-ion) that optimizes LF violation would adopt equatorial settings by default. The gap is structural, not coincidental — it would persist regardless of how many optical EWF implementations exist. The two approaches are complementary: LF optimization maximizes inequality violation at fixed θ; this work varies θ to test for overlap-dependent deformation. The single-waveplate protocol preserves the optimized LF violation (8.6σ) while adding the θ degree of freedom — combining both tests in one experiment.

Protocol motivation. The scarcity of optical EWF implementations — precisely two in two decades — makes a low-cost protocol especially well-matched to the experimental landscape. A dedicated new EWF experiment requires years of design, funding, and construction; a single-waveplate modification runs on existing hardware in approximately one hour (§IV E). Tilting the Superobserver opens access to this previously untested sector (§IV).

IV. EXPERIMENTAL PROTOCOL (CLAIM B)

A. Breaking the Cancellation

Any $\theta \neq \pi/2$ breaks the cancellation. A grid search over $(\theta, \phi_2, \phi_3, \beta_{\text{Bob}})$ maximizing $\text{FOM}(\theta, \beta, N) = \min(n_\sigma^{\text{LF}}, n_\sigma^{\text{signal}})$ with $\beta = 0.30$ yields a broad plateau peaking near $\theta \approx 31°$–$35°$ (FOM = 8.6–8.8). At $\beta = 0.30$, $n_\sigma^{\text{signal}} \gg n_\sigma^{\text{LF}}$ across all θ, so the FOM is bounded by n_σ^{LF}. Representative FOM values at $\mu = 0.95$, $\beta = 0.30$ (per-θ angle re-optimization, Supplemental S2): 5.8 ($\theta = 20°$), 8.6 ($\theta = 31°$), 8.8 ($\theta = 35°$), 6.0 ($\theta = 45°$), 0 ($\theta = 58°$, Gen LF 1 becomes negative), and 0 ($\theta = 90°$, cancellation); FOM $> 5\sigma$ for $\theta \in [20°, 45°]$. At $\beta \approx 0.07$ (single-setting, just below the single-setting 5σ threshold $\beta \approx 0.075$), the FOM is signal-limited: optimal $\theta = 46°$ (FOM = 5.4) and single-setting $> 5\sigma$ range $\theta \in [35°, 46°]$ (Supplemental S2). The reference angle $\theta = 31°$ gives single-setting significance 4.7σ at $\beta = 0.07$; reaching 5σ there requires $\beta \gtrsim 0.075$ (single-setting) or combining the four mixed settings (9.4σ at $\beta = 0.07$, §V C). The $\beta = 0.30$ plateau $\theta \in [20°, 45°]$ does include $\theta = 31°$.

The wide optimal window means the protocol tolerates angular misalignment of $\pm 11°$ before dropping below 5σ — substantially more forgiving than the alignment precision demanded by the standard Bong protocol.

The optimum at $\theta \approx 31°$–$35°$ reflects how the two significances vary with θ. In this tilted-Superobserver geometry the Gen LF 1 violation is itself maximized at an intermediate tilt: it weakens as $\theta \to 0°$ (settings 2,3 collapse onto the z-basis of setting 1, removing the angular spread the Facet 1 inequality requires) and also weakens toward the equator, the achievable violation falling to zero near $\theta \approx 55°$ (Gen LF 1 turns negative by $\theta \approx 58°$; Supplemental S2 grid search). The overlap signal independently vanishes at $\theta = 90°$ (equatorial cancellation, §III) and is non-zero otherwise. At $\beta = 0.30$ the FOM is LF-limited, so its $\theta \approx 31°$–$35°$ plateau tracks the peak of the Gen LF 1 violation; at $\beta \approx 0.07$ the FOM is signal-limited and the optimum shifts toward $\theta \approx 46°$. The exact location is set by the Gen LF 1 inequality coefficients via grid search (Supplemental S2). The broad plateau (FOM $> 5\sigma$ for $\theta \in [20°, 45°]$ at $\beta = 0.30$) means the exact optimum is not critical — any angle in this range produces a viable experiment. We adopt $\theta = 31°$ as the reference angle throughout because it coincides with the QWP-determined tilt in the Bong apparatus.

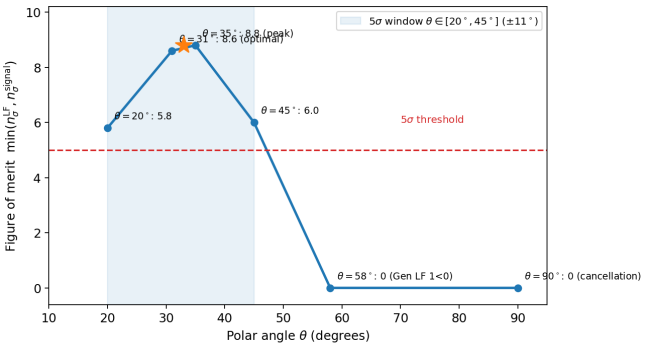

FIG. 2. Figure of merit vs polar angle θ, showing plateau near $\theta \approx 31°$–$35°$ ($\beta = 0.30$) and 5σ detection boundary spanning $\theta \in [20°, 45°]$.

Gen LF 1(θ) and $\delta\langle AB\rangle(\theta)$ are independent observables from the same coincidence data. Gen LF 1 aggregates all eleven correlators; its θ-dependence is a standard QM prediction — LF violation weakens as measurement axes approach a common direction. $\delta\langle AB\rangle$ isolates deviations of individual mixed-setting correlators from their QM expectation. A shift in Gen LF 1 without the θ-dependent pattern in $\delta\langle AB\rangle$ would indicate apparatus misalignment, not β; conversely, $\delta\langle AB\rangle \neq 0$ with Gen LF 1 matching its QM prediction is the signature of overlap-dependent physics (Table VII). The ϕ-scramble control (§VII) provides additional discrimination.

B. Single Hardware Modification

In standard Bong et al. (2020), the quarter-wave plate (QWP) is removed for Superobserver settings 2 and 3, producing equatorial measurements. Our modification re-inserts this same QWP into Superobserver Alice's measurement path (before the PBS, after beam dis-

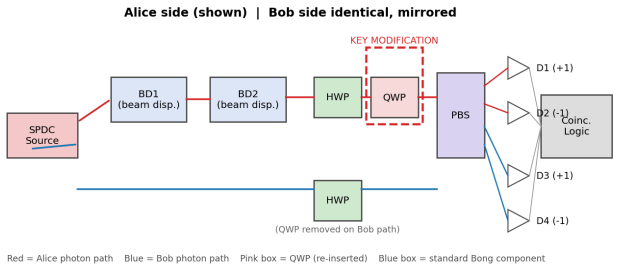

FIG. 3. Optical path with QWP insertion highlighted.

placer BD2), tilting the effective measurement axis to $\theta = 31°$. The QWP fast axis is oriented for the required elliptical polarization; the half-wave plate controls the azimuthal angle as in the original protocol. QWP specifications (retardance tolerance, temperature stability) and angular uncertainty analysis are provided in Supplemental S2. This is the only optical hardware change required. (The SNSPD upgrade discussed in §VII replaces existing detectors at the same optical position; no new optical elements are introduced.) A ϕ-scramble control (§VII) randomizes the azimuthal angle to rule out birefringence artifacts without additional optics.

C. Measurement Settings

TABLE III. Measurement settings: standard Bong et al. (2020) vs. this work.

Parameter	Standard Bong [2]	This Work
Polar angle θ	90° (equatorial)	**31°**
Alice ϕ_2	0°	**112°**
Alice ϕ_3	118°	**217°**
Bob β_{Bob}	175°	**20°**
μ required (onset)	not specified	≥ 0.86
N	91,000	91,000

D. Calibration

1. Verify polar angle: $|\langle\sigma_z\rangle| = \cos(31°) \approx 0.857$ on H-polarized state (± 0.01).

2. Verify azimuthal alignment with entangled state (count rates within 2% of QM).

3. Measure μ via CHSH S-parameter ($\mu \geq 0.86$ required for LF violation onset).

E. Practical Feasibility

Bong et al. (2020) report ∼1000 coincidence events per second. At this rate, $N = 91{,}000$ per setting requires ∼91 s of integration; nine setting combinations plus calibration (θ-verification and azimuthal alignment checks) would require a data-acquisition run of approximately one hour under Bong et al. conditions, assuming source and detector stability over this timescale. Practical feasibility depends on the specific apparatus; detailed acquisition timing and stability estimates are provided in Supplemental S2.

V. MODEL-INDEPENDENT QM PREDICTIONS

All numerical values are computed from the density matrix $\rho_\mu = \mu|\Psi^-\rangle\langle\Psi^-| + (1-\mu)(|HV\rangle\langle HV| + |VH\rangle\langle VH|)/2$ for the singlet state with visibility $\mu = 0.95$. SPDC produces photon pairs only in the $\{|HV\rangle, |VH\rangle\}$ subspace; the noise term is the maximally mixed state within that subspace, not the full $I/4$.

A. Correlators at $\theta = 31°$, $\mu = 0.95$

All nine $\langle A_x B_y\rangle$ correlators are tabulated in Supplemental S2. Key values: $\langle A_1 B_1\rangle = -1.0000$ (z-basis, perfect anti-correlation); mixed-setting correlators range from $\langle A_2 B_2\rangle = -0.5045$ to $\langle A_2 B_3\rangle = \langle A_3 B_2\rangle = -0.8933$, all with $\sigma \approx 0.0017$ at $N = 91{,}000$. The four mixed-setting pairs (one side z-basis, one side tilted) share identical $|\langle AB\rangle|$ up to ϕ-induced sign, since $f_\perp$ depends only on θ. Standard QM predicts zero marginals (singlet, $\mu = 0.95$).

B. Primary Observable: Genuine LF Violation

TABLE IV. Genuine LF violation prediction.

Observable	Prediction	Type
Gen LF 1	$+0.0891 \pm 0.0103$ (8.6σ)	Standard QM, model-independent

The 8.6σ LF violation provides built-in calibration: no violation at $\geq 5\sigma$ indicates the apparatus is not realizing the intended geometry.

C. Sensitivity to Overlap-Dependent Deformations

The figure of merit governing experimental sensitivity is $\text{FOM}(\theta, \beta, N) = \min(n_\sigma^{\text{LF}}(\theta, N), n_\sigma^{\text{signal}}(\theta, \beta, N))$, where $n_\sigma^{\text{LF}} = |\text{Gen LF } 1(\theta)|/\sigma_{\text{LF}}$ is the LF violation significance (§IV A, Eq. 1) and $n_\sigma^{\text{signal}} = |\delta\langle AB\rangle|/\sigma_{AB}$ is the overlap-dependent signal significance, with $\sigma_{AB} = \sqrt{[(1 - \langle AB\rangle^2)/N]}$ (§VI). The optimum at $\theta = 31°$ reported in §IV A maximizes this FOM via grid search.

For Eq. (2)–(3), we compute $\delta\langle A_x B_y\rangle = \langle A_x B_y\rangle_{\text{model}} - \langle A_x B_y\rangle_{\text{QM}}$ by exact numerical integration over the density matrix. The computation evaluates $f_\perp$-weighted outcome probabilities with full renormalization (see Supplemental S2 for the numerical method). Results for the mixed settings (one side z-basis, one side tilted) at $\theta = 31°$, $\mu = 0.95$:

TABLE V. Sensitivity to outcome-dependent coupling β.

β	$\lvert\delta\langle AB\rangle\rvert$ (mixed)	n_σ (single setting, N=91k)	n_σ (4 combine
0.03	0.0034	2.0	4.0
0.05	0.0057	3.3	6.7
0.07	0.0080	4.7	9.4
0.10	0.0115	6.7	13.5
0.30	0.0355	20.8	41.6

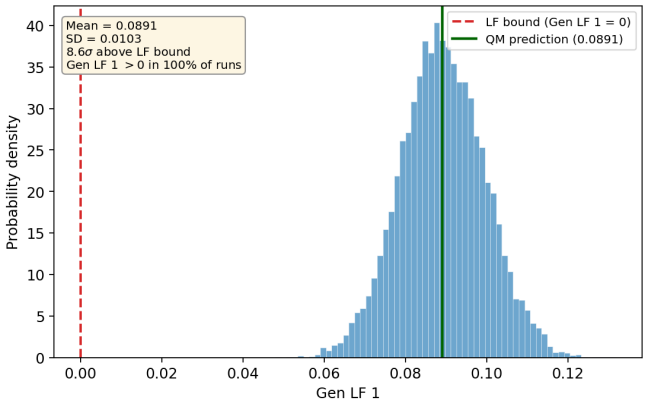

FIG. 4. Monte Carlo histogram of Gen LF 1.

All four mixed settings yield identical δ ($f_\perp$ depends only on θ, not ϕ).

For Eq. (2)–(3), the illustrative 5σ detection threshold is $\beta \sim 0.07$ (single-setting, $N = 91{,}000$). Using all four mixed settings combined, $\beta \sim 0.04$ is detectable at $>5\sigma$ ($\beta_{\min} \approx 0.038$ under idealized Poisson statistics; see §VI). Accounting for realistic systematics (§VI–VII), the practical sensitivity floor is likely $\beta \sim 0.05$–0.10 (single-setting) and $\beta \sim 0.04$–0.06 (combined). These thresholds are illustrative — no existing theory predicts a specific β value; they quantify the experiment's capability for Eq. (2)–(3).

Experimental discriminator. Standard QM predicts $\delta\langle AB\rangle = 0$ for all θ. Eq. (2)–(3) predicts $\delta\langle AB\rangle = 0$ at $\theta = \pi/2$ (equatorial cancellation) and $\delta\langle AB\rangle \neq 0$ for $\theta \neq \pi/2$, with exact θ-dependence determined numerically (the unrenormalized leading-order structure goes as $\cos\theta$, but renormalization modifies the functional form; see Supplemental S2). This signature is testable by θ-sweep (§VIII) and is not a reparameterization of QM: it is distinct from conventional systematics (which either cancel in $\delta\langle AB\rangle$ or produce non-geometric θ-dependence), making a θ-dependent $\delta\langle AB\rangle$ signal difficult to reproduce without overlap-dependent physics (Lemma 1, §III C).

β in context. The coupling β has no a priori prediction — analogous to SME coefficients at inception (see §II C for the methodological parallel). For scale reference: photon-sector SME coefficients are constrained to $<10^{-23}$ [15]; continuous spontaneous localization (CSL) collapse parameters are bounded at $\lambda \approx 10^{-16}\,\text{s}^{-1}$; weak-measurement anomaly searches constrain postselection deviations at $\sim 10^{-2}$ [18]. A constraint $\beta \geq 0.04$ would place overlap-dependent deformation in the company of these phenomenological parameter classes — opening a new parameter space at the $\sim 10^{-2}$ scale (comparable to weak-measurement anomalies) while distinct from SME and collapse regimes in both scale and physical mechanism. A null result at $\beta \geq 0.04$ excludes $O(1)$ and $O(10^{-1})$ deformation for the class Eq. (2)–(3); a positive result provides the first quantitative target for theory construction. Increasing to $N = 200{,}000$ extends sensitivity to $\beta \geq 0.02$. The $\sim 10^{-2}$ scale is physically motivated: postselection-conditioned weak values [18] manifest at the same order, and any overlap-dependent structure would naturally appear at the precision where measurement-context effects become distinguishable from Poisson noise in current optical implementations.

The gap between $\beta_{\min} \approx 0.038$ (combined) and $\beta_{\min} \approx 0.075$ (single setting) reflects the $\sqrt{4} = 2$ improvement from combining four independent measurements. The experiment naturally provides all four mixed-setting correlators; no additional data acquisition is needed for the combined analysis.

VI. STATISTICAL ANALYSIS

Poisson statistics: $\sigma(\langle A_x B_y\rangle) = \sqrt{[(1 - \langle A_x B_y\rangle^2)/N]}$. For Gen LF 1 (11 terms, coefficients up to ± 2): $\sigma(S_{\text{LF1}}) = \sqrt{\sum_i c_i^2 (1 - \langle v_i\rangle^2)/N} \approx 0.0103$ at $N = 91{,}000$ (exact term-by-term propagation; the upper bound $\sqrt{20}/\sqrt{N} \approx 0.015$ assumes all correlators near zero).

Minimum sample for 5σ LF detection: $N_{\min} \approx 30{,}800$. $N = 91{,}000$ provides a factor of 3 margin.

Monte Carlo (10,000 runs): Gen LF 1 $\geq 5\sigma$ in 99.97%; $\beta = 0.07$ detected in $\sim 38\%$ at 5σ (single setting, $n_\sigma = 4.7$; see §V C), $>99\%$ (four combined settings, $n_\sigma = 9.4$); $\beta = 0.05$ in $\sim 90\%$ at 5σ (combined, $n_\sigma = 6.7$). A conservative Bayesian analysis inflating Poisson uncertainties by 20% yields $\beta_{\min} \approx 0.046$ (combined); the FOM plateau (§IV A: $>5\sigma$ for $\theta \in [20°, 45°]$) ensures viability under substantial systematic degradation. Detailed Monte Carlo, correlated-drift modeling, and fake-signal injection methodology are provided in Supplemental S2.

VII. ROBUSTNESS SUMMARY

The experiment is robust under realistic Bong et al. (2020) conditions. Required loophole-closed 5σ detec-

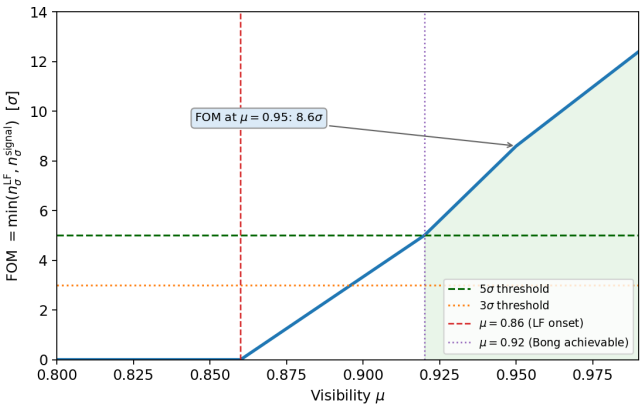

FIG. 5. FOM vs. μ.

tion thresholds (visibility $\mu \geq 0.92$, efficiency $\eta \geq 0.91$) are within reach (Bong achieved $\mu = 0.92$, $\eta = 0.87$; SNSPD upgrade [16] closes the detection loophole). A six-source systematic-error budget finds all contributions sub-dominant to Poisson noise ($\sigma \approx 0.0017$ at $N = 91{,}000$):

TABLE VI. Systematic-error budget.

Systematic source	Controlled by	vs. Poisson
QWP retardance	Retardance tolerance	<1
Birefringence	ϕ-scramble control (see below)	<1
Polarization-dependent loss	Power monitoring per channel	<1
Calibration offset	θ-verification protocol (§IV D)	<1
Detector asymmetry	Channel efficiency balancing	<1
Accidentals	Timing windows + dark-count subtraction	<1

RSS total remains below the Poisson floor. Exact σ values and Monte Carlo correlation analysis in Supplemental S2. A ϕ-scramble control ($N_\phi \geq 10$, fit $\delta\langle AB\rangle(\phi) = A + B\cos(2\phi) + C\sin(2\phi)$) distinguishes geometric θ-dependent signal ($A \neq 0$, $B, C \approx 0$) from birefringence artifacts (B or $C \neq 0$) at the 5σ level. Detector inefficiency cannot fake a β signal: residual θ-dependent efficiency biases δ toward zero [9].

Two-phase experimental program. Phase 1 (near-term, $\eta \approx 0.87$): a loophole-open screening test using existing hardware plus one QWP, constraining $\beta \sim 0.07$ under fair-sampling. Phase 2 (loophole-closed, $\eta \geq 0.91$ via SNSPD upgrade [16]): same optical configuration, only the detectors change — closes the detection loophole with no redesign. Full robustness analysis in Supplemental S2.

VIII. DISCUSSION

A. Interpretation and Falsification

A non-zero $\delta\langle AB\rangle$ at $\theta = 31°$ would demonstrate Superobserver-Friend correlations departing from standard QM at a previously untested geometry. The overlap-only class is definitively falsified if: (i) a θ-sweep over the pre-registered angle set $\{20°, 31°, 35°, 45°, 58°\}$ shows $\delta\langle AB\rangle = 0$ at all these non-equatorial angles to within ± 0.003 ($90°$ serves as the equatorial control; statistical floor at $N = 200{,}000$ per setting); or (ii) $\delta\langle AB\rangle(\theta)$ is non-zero at $\theta = \pi/2$ (violating the equatorial cancellation theorem) after accounting for systematics. Either outcome is informative: falsification closes the overlap-only window; a θ-dependent signal opens it.

TABLE VII. Observable predictions: Standard QM vs. overlap-only model.

Observable	Standard QM	Overlap-only (Eq. 2–3)
Gen LF 1 at $\theta = 31°$	$+0.0891 \pm 0.0103$ (8.6σ)	Same (LF violation preserved)
$\delta\langle AB\rangle$ at $\theta = 31°$	0	$\approx 0.115\beta$ (numerical)
$\delta\langle AB\rangle$ at $\theta = \pi/2$	0	0 (equatorial cancellation, exact)
$\delta\langle AB\rangle(\theta)$ functional form	$\delta = 0\ \forall\theta$	$\delta = 0$ iff $\theta = \pi/2$; non-zero otherwise (exact form numerical)

A null result at Level 0 ($\beta < \beta_{\min}$ across the full θ-sweep) falsifies the overlap-only class but leaves Levels 1–3 unconstrained: density-matrix-dependent (ρ_F), multipartite (concurrence), and non-geometric (timing, path) deformations are not bounded by Proposition 1 and each requires independent experimental designs.

B. Future Directions

θ-sweep. A systematic scan over the pre-registered angle set $\{20°, 31°, 35°, 45°, 58°, 90°\}$ ($90°$ = equatorial control) would directly map the θ-dependence of $\delta\langle AB\rangle$ predicted by Eq. (2), testing for the equatorial zero ($\delta = 0$ at $\theta = 90°$) and non-zero signal at $\theta \neq 90°$. To prevent analysis bias, the sweep should be performed blind (randomized θ sequence, analysis finalized before unmasking). A null result across all θ excludes the overlap-only class to $\beta \approx 0.02$ ($N = 200{,}000$ per setting).

Multi-observer extension. Extension to $N > 2$ observers is a natural next step; the geometric cancellation condition generalizes to multi-observer overlap products and is left for future work.

Platform independence. The theorem in §III is platform-agnostic. Implementing tilted Superobserver measurements on solid-state or trapped-ion platforms

would test whether the $\cos\theta$ structure persists when the Friend is a macroscopic quantum system.

Locality closure. Combining the tilted geometry with space-like separated random basis switching would close the locality loophole alongside the detection loophole (§VII), representing a natural next-generation experiment.

IX. CONCLUSION

All published optical EWF implementations have operated at an equatorial fixed point ($\theta = \pi/2$) where every overlap-dependent deformation vanishes identically (Proposition 1), leaving the overlap-only class systematically unexplored within the surveyed literature (Supplemental S1).

We propose a null test to probe this class: re-insert one QWP into the Bong et al. (2020) apparatus ($\theta = 31°$), providing sensitivity $\beta \sim 0.075$ at 5σ (single-setting) while preserving 8.6σ LF violation. The experiment requires no new technology — only re-insertion of an existing waveplate — and would open the first experimental window onto overlap-dependent physics in EWF scenarios.

[1] M. Proietti *et al.*, Sci. Adv. **5**, eaaw9832 (2019).
[2] K. W. Bong *et al.*, Nat. Phys. **16**, 1199–1205 (2020).
[3] E. P. Wigner, in *The Scientist Speculates* (Heinemann, 1961).
[4] D. Deutsch, Int. J. Theor. Phys. **24**, 1–41 (1985).
[5] L. Hardy, Phys. Rev. Lett. **68**, 2981 (1992).
[6] D. Frauchiger and R. Renner, Nat. Comms. **9**, 3711 (2018).
[7] N. Brunner *et al.*, Rev. Mod. Phys. **86**, 419 (2014).
[8] J. S. Bell, Physics **1**, 195–200 (1964).
[9] M. Giustina *et al.*, Phys. Rev. Lett. **115**, 250401 (2015).
[10] H. M. Wiseman, E. G. Cavalcanti, and E. G. Rieffel, Quantum **7**, 1112 (2023).
[11] M. Haddara and E. G. Cavalcanti, arXiv:2407.20346 (2024).
[12] A. Utreras-Alarcon, E. G. Cavalcanti, and H. M. Wiseman, Proc. R. Soc. A **480** (2023).
[13] M. Haddara and E. G. Cavalcanti, New J. Phys. **25**, 093028 (2023).
[14] A. Kent, arXiv:2302.12707 (2023).
[15] D. Colladay and V. A. Kostelecký, Phys. Rev. D **55**, 6760 (1997).
[16] F. Marsili *et al.*, Nat. Photonics **7**, 210–214 (2013).
[17] J. Barrett, Phys. Rev. A **75**, 032304 (2007).
[18] Y. Aharonov, D. Z. Albert, and L. Vaidman, Phys. Rev. Lett. **60**, 1351 (1988).